THE JOURNAL OF PHYSICAL CHEMISTRY A

Article

pubs.acs.org/JPCA

Thermal Decomposition of 1-Pentanol and Its Isomers: A Theoretical Study

Long Zhao, Lili Ye, Feng Zhang,* and Lidong Zhang*

National Synchrotron Radiation Laboratory, University of Science and Technology of China, Hefei, Anhui 230029, P. R. China

Supporting Information

ABSTRACT: Pentanol is one of the promising "next generation" alcohol fuels with high energy density and low hygroscopicity. In the present work, dominant reaction channels of thermal decomposition of three isomers of pentanol: 1-pentanol, 2-methyl-1-butanol, and 3-methyl-1-butanol were investigated by CBS-QB3 calculations. Subsequently, the temperature- and pressure-dependent rate constants for these channels were computed by RRKM/master equation simulations. The difference between the thermal decomposition behavior of pentanol and butanol were discussed, while butanol as another potential alternative alcohol fuel has been extensively studied both experimentally and theoretically. Rate constants of barrierless bond dissociation reactions of pentanol isomers were treated by the variational transition state theory. The comparison between various channels revealed that the entropies of variational transition states significantly impact the rate constants of pentanol decomposition reactions. This work provides sound quality kinetic data for major decomposition channels of three pentanol isomers in the temperature range of 800−2000 K with pressure varying from 7.6 to 7.6 × 10^4 Torr, which might be valuable for developing detailed kinetic models for pentanol combustion.

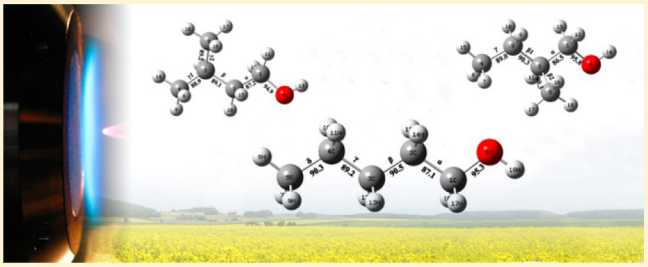

1. INTRODUCTION

As a suitable alternative of fossil fuel, biofuel such as bioalcohol, biodiesel, and biogas, which are derived from biomass, has attracted great interest among scientists and government policy makers. Compared with the "first generation" alcohol fuels, i.e., methanol and ethanol, the "next generation" alcohol fuels such as butanol and pentanol exhibit better combustion properties including greater energy density and lower hygroscopicity.[1,2] Recently, pentanol and its isomers (2-methyl-1-butanol and 2-methyl-1-butanol) were considered as potential biofuels.[3,4] The intelligent use of biofuel requires understanding the mechanism of the pyrolysis, oxidation, and combustion processes. Further, detailed chemical kinetic modeling for biofuel combustion needs accurate kinetic studies for these fuels.

Numerous studies have been performed on the combustion behavior of methanol and ethanol due to their long history. Butanol as a "next generation" alcohol fuel has attracted much attention in the combustion community over the last five years. For example, lots of experimental studies have been performed on the pyrolysis, oxidation, and flame of isomeric butanols under various experimental conditions,[5−9] theoretical calculations were also employed to compute the potential energy surfaces (PESs) and rate constants of important reaction channels involved in butanol combustion.[10−14] Consequently, chemical kinetic models for butanol combustion have been constructed by several research groups to accommodate different combustion conditions.[6,7,9,10,15,16] Compared to the exhaustive studies on butanol combustion, studies on pentanol combustion are very limited. In 2004, Mellouki et al. measured the rate constants of OH radical reacting with 3-methyl-1-butanol and 3-methyl-2-butanol at low temperature (241−373 K).[17] Welz and co-workers investigated the low temperature (550−750 K) oxidation mechanism of isopentanol by using time-resolved tunable synchrotron photoionization mass spectrometry.[18] Very recently, Togbé and co-workers first reported detailed kinetic models for *n*-pentanol and isopentanol based on jet stirred reactor (JSR) experiments.[19,20] To the best of our knowledge, no computational results are available for the thermal decomposition and oxidation mechanism of pentanol and its isomers, although they are important for understanding the combustion chemistry of pentanol as a potential biofuel and for constructing accurate kinetic models of pentanol combustion.

In the present work, dominant channels of thermal decomposition of 1-pentanol and two of its isomers (2-methyl-1-butanol and 3-methyl-1-butanol) were investigated by ab initio methods. The corresponding rate constants were computed considering the dependence of temperature and pressure. In order to explore the difference between the thermal decomposition behavior of butanol and pentanol, we compared our calculated bond dissociation enthalpies (BDEs) of the three pentanol isomers with those of 1-butanol and 2-butanol.[11] Furthermore, we computed the temperature -(800−2000 K) and pressure-dependent (7.6 to 7.6 × 10^4 Torr) rate constants

Received: June 15, 2012
Revised: August 15, 2012
Published: August 21, 2012

of major reaction channels of pentanol decomposition with the RRKM/master equation method, providing reference data for kinetic modeling study of pentanol combustion

2. COMPUTATIONAL DETAILS

2.1. Ab Initio Methods. The unimolecular decomposition pathways were calculated with the CBS-QB3 method, which is a composite method starting from a geometry optimization at B3LYP/6-311G(2d,d,p) followed by a series of high level single-point energy corrections including the complete basis set extrapolation.[21,22] For the barrierless bond fission reactions, the reaction systems exhibit substantial multireference character in the region of chemical bond elongation. Thus, the minimum energy potentials (MEPs) for these reactions were constructed by a relaxed scan along the reaction coordinates (i.e., the breaking bond) with the stepsize of 0.2 Å at the CASPT2(2e,2o)/6-311G(d,p)//CASSCF(2e,2o)/6-311G(d,p) level. The active space was chosen as the bonding orbital σ and antibonding orbital σ^* for the breaking bonds. The potential energy curve at CASPT2 was fitted into a Morse potential $V(r) = D_e(1 - e^{-\alpha(r-r_e)})^2$, where D_e refers to the dissociation energy. Then, this dissociation energy at CASPT2 was scaled by the computed dissociation energies at CBS-QB3; consequently, the complete potential energy curve was scaled. All the calculations were performed with the Gaussian03 program.[23]

Bond dissociation enthalpies were evaluated from the standard enthalpies of formation in the gas phase ($\Delta H^0_{298,f}$), which were computed using the atomization energy approach.[11] In brief, the standard enthalpy of formation for the molecule M with N atoms is computed by the following formula:

$$\Delta H^0_{298,f}(M) = E_e(M) + \mathrm{ZPE}(M) + [H_{298}(M) - H_0(M)] - \sum_{i=1}^{N}\{E_e(X_i) + [H_{298}(X_i) - H_0(X_i)]\} + \sum_{i}^{N}\Delta H^0_{298,f}(X_i) \quad (1)$$

where E_e is the electronic energy, ZPE is the zero-point vibrational energy of the molecule, $[H_{298}(M) - H_0(M)]$ is the thermal correction to the enthalpy, and X_i refers to the ith atom (C, H, and O in this work). The atomic enthalpies $\Delta H^0_{298,f}(X_i)$ can be found in the NIST chemistry WebBook.[24]

2.2. Rate Constants Calculations. The pressure- and temperature-dependent rate constants were computed with the RRKM/master equation method using ChemRate program.[25] The temperature ranges from 800 to 2000 K, and the pressure varies from 7.6 to 7.6 × 10^4 Torr. The bond fission channels without apparent transition state were treated variationally in the temperature range by the computation procedure proposed by da Silva et al. using ChemRate.[26] In brief, the high pressure limit (HPL) rate constant was calculated as a function of temperature and position of the transition state, i.e., $k_{HPL}(T)$ was calculated at each point along the reaction coordinate. At each temperature, the variational transition state is located as the geometry with the minimum $k_{HPL}(T)$. The low-frequency vibrational modes corresponding to internal rotation around the breaking bonds were assumed as free rotors. Other torsional modes were dealt with the hindered rotor approximation based on the hindrance potentials computed at the B3LYP/6-31 g(d) level. All hindrance potentials were assumed symmetric, while the highest barrier heights of the asymmetric hindrance potentials were used to compute the partition functions of hindered rotors. Tunneling effect was ignored in this work since all reactions studied involve the movement of relatively heavy atoms (C or O); furthermore, the interested temperatures in this work are quite high.

The interaction between reactants and the bath gas Ar was modeled by the Lennard-Jones (L-J) potential. The Lennard-Jones parameters for Ar and pentanol were computed with the following empirical equations:[27]

$$\sigma = 2.44(T_c/P_c)^{1/3} \quad (2)$$

$$\varepsilon_A/k_b = 0.77T_c \quad (3)$$

where k_b is the Boltzmann constant. The critical temperature (T_c) and pressure (P_c) were cited from the NIST database. The L-J parameters were then computed as σ = 6.000 Å, ε = 446.6 K for 1-pentanol; σ = 5.964 Å, ε = 443.06 K for 2-methyl-1-butanol; and σ = 5.908 Å, ε = 445.8 K for 3-methyl-1-butanol according to eqs 2 and 3. For Ar, the collisional parameters are σ = 3.548 Å, ε = 116 K. The collision energy transfer was treated using a single-parameter exponential down model. The average energy transferred in deactivating collisions, i.e., $\langle\Delta E_{down}\rangle$, was taken to be proportional to the temperature with the proportionality coefficient of 0.8 cm^{-1}/K.

Equilibrium constants in terms of partial pressure were calculated by $K_p = \exp(-\Delta G/RT)$, where R is the ideal gas constant with 82.057 cm^3 atm mol^{-1} K^{-1}, and ΔG is the standard Gibbs free energy change at CBS-QB3 in this work. The base 10 logarithms of equilibrium constants $K_p(T)$ were given by the ChemRate program.[25] The relationship between equilibrium constant in terms of partial pressure (K_p) and concentration (K_c) is $K_c = K_p(RT)^{-\Delta n}$, where Δn refers to the number of moles of gaseous products.

3. RESULTS AND DISCUSSION

3.1. Geometries and Bond Dissociation Enthalpies. The primary thermal decomposition channels of pentanol include C−C, C−O, C−H, and O−H bond dissociation and H_2O-elimination reactions. With the knowledge of the known BDEs and rate constants on smaller alcohols, the cleavage of C−H and O−H bonds should not compete with the other two bond dissociation channels.[11,28−30] In addition, among possible small molecule (e.g., H_2, CH_4, etc.) elimination reactions for alcohols, the H_2O-elimination always has the lowest barrier height; the energy difference between the H_2O elimination and other small molecule elimination reactions is usually larger than 10 kcal/mol. Therefore, in this work, we only calculate the PESs and rate constants of the C−C and C−O bond dissociation reactions and the H_2O elimination reaction. In order to check the performance of CBS-QB3 method for studied systems, the calculated standard enthalpies of formation in the gas phase were compared with the experimental values, which were provided by the NIST database. The $\Delta H^0_{298,f}$ calculated by 1 at CBS-QB3 for 1-pentanol (RC1) is −69.9 kcal/mol, while the experimental value is −69.6 kcal/mol; the calculated $\Delta H^0_{298,f}$ for 2-methyl-1-butanol (RC2) is −71.5 kcal/mol versus the experimental value −72.2 kcal/mol, and the $\Delta H^0_{298,f}$ at CBS-QB3 for 3-methyl-1-butanol (RC3) is −71.1 kcal/mol, while the experimental value is −71.9 kcal/mol. All deviations are within 1 kcal/mol.

Figure 1 shows the optimized geometries at B3LYP/6-311G(2d,d,p) of RC1, RC2, and RC3 and the calculated BDEs at 298 K at CBS-QB3 level for C−C and C−O bonds. The

dx.doi.org/10.1021/jp305885s | J. Phys. Chem. A 2012, 116, 9238−9244

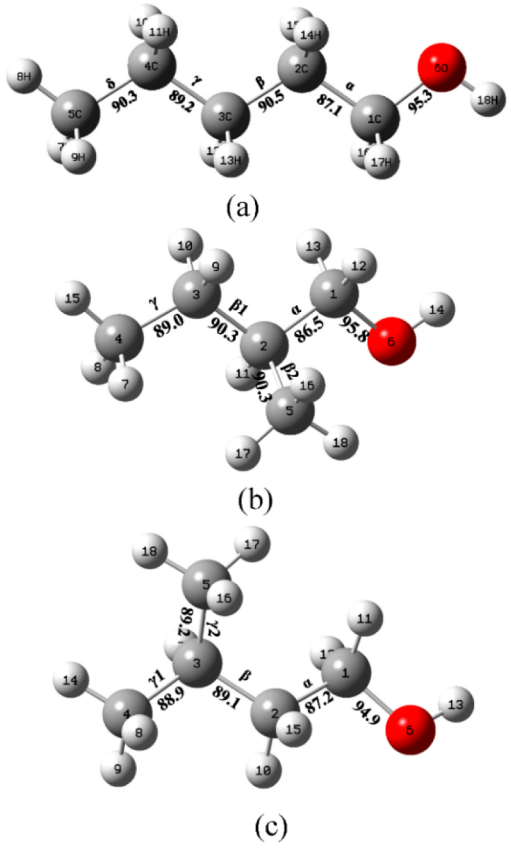

Figure 1. Optimized geometries at B3LYP/6-311G(2d,d,p) for 1-pentanol (a), 2-methyl-1-butanol (b), and 3-methyl-1-butanol (c). The number below each bond is the calculated BDE at 298 K at the CBS-QB3 level.

BDEs of the α C−C bond for all three isomers have the lowest values, which are almost 2 kcal/mol higher than the nearest BDEs and 7.7−9.3 kcal/mol higher than the BDEs of C−O bonds. It indicates that the C−O cleavage may not be comparable with the C−C bond cleavage, even at high temperature, e.g., 800−2000 K. Table 1 listed the BDEs at

Table 1. Calculated BDEs at CBS-QB3 for C1−C5 Primary Alcohols

	bond dissociaton energy at 298 K (kcal/mol)				
primary alcohols	C−O	α C−C	β C−C	γ C−C	δ C−C
C1 (methanol)[a]	93.2				
C2 (ethanol)[a]	95.3	88.0			
C3 (1-propanol)[a]	95.4	86.2	91.0		
C4 (1-butanol)[a]	95.2	87.5	90.0	90.0	
C5 (1-pentanol)[b]	95.3	87.1	90.5	89.2	90.3

[a]Cited from ref 11. [b]This work.

CBS-QB3 for the C−O and C−C bonds in the C1−C5 primary alcohols, in which the results for C1−C4 alcohols were calculated by EI-Nahas with the same methods.[11] In general, the BDEs are influenced by both the position of the breaking bond (α, β, γ, etc.) and the primary/secondary/tertiary carbon atom connected. Table 1 does not show apparent correlation between the calculated BDEs of C−O and C−C bonds and the chain length. The Cartesian coordinates of the geometries in Figure 1 are given in the Supporting Information.

3.2. Decomposition Pathways. Figures 2−4 display the potential energy profiles for major decomposition pathways of

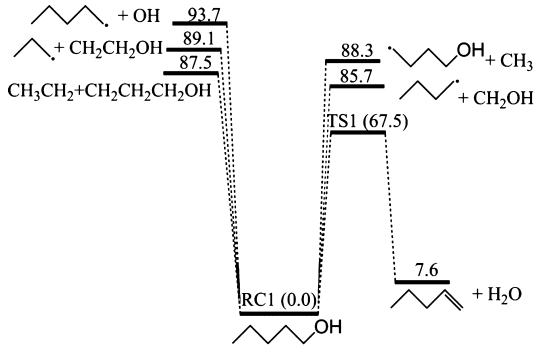

Figure 2. Potential energy profiles at CBS-QB3 for the major unimolecular decomposition channels of 1-pentanol (RC1).

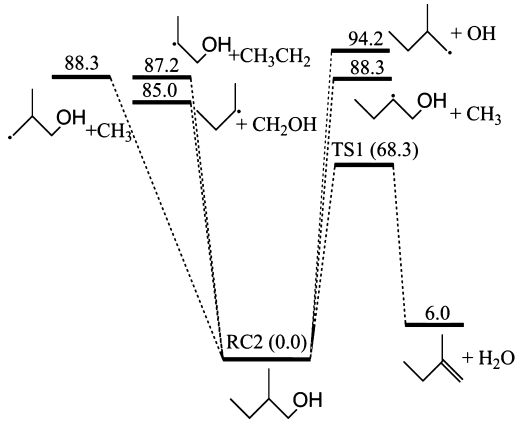

Figure 3. Potential energy profiles at CBS-QB3 for the major unimolecular decomposition channels of 2-methyl-1-butanol (RC2).

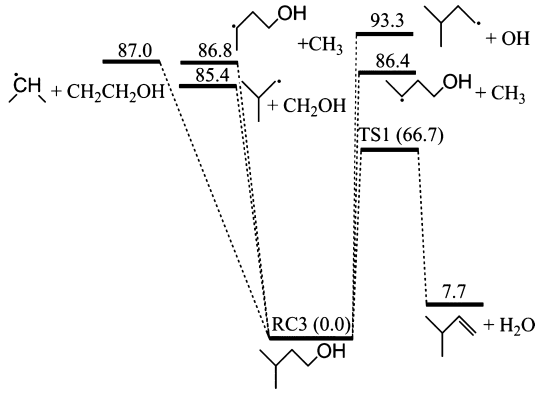

Figure 4. Potential energy profiles at CBS-QB3 for the major unimolecular decomposition channels of 3-methyl-1-butanol (RC3).

RC1, RC2, and RC3, i.e., the C−C and C−O bond dissociation and the H_2O elimination, as mentioned previously. Clearly, the C−O bond dissociation has the highest bond dissociation energy, varying from 93.3 to 94.2 kcal/mol for each isomer. The α C−C bond fission needs the lowest energy among all direct bond dissociation pathways; the corresponding bond dissociation energy is around 85.0 kcal/mol for each molecule. However, the dissociation energies of other C−C bonds are quite close to that of α C−C bond, especially for RC3, the highest bond dissociation energy (β C−C) is only 1.6 kcal/mol

dx.doi.org/10.1021/jp305885s | J. Phys. Chem. A 2012, 116, 9238−9244

higher than that of α C−C bond. Compared with RC1 and RC2, whose highest C−C bond dissociation energies are 3.3−3.4 kcal/mol higher than the dissociation energy of the α C−C bond, the small energy difference of C−C bond dissociation energies for RC3 is due to the high stability of isopropyl radical. The transition states of H_2O elimination for RC1 through RC3 have the lowest barrier heights, which are less than 70 kcal/mol. Although the barrier heights of H_2O elimination are much lower (16.7−18.7 kcal/mol) than the lowest dissociation energies of C−C bonds dissociation for all the three molecules, it is hard to conclude the competition between these reaction channels without further kinetic calculations. It will be discussed later.

Required by the variational TST calculations, the step-wisely optimized potential energy curve along the breaking bond length is constructed by the multireference method and then multiplied by a scale factor according to the CBS dissociation energy, as described in section 2. The scale factors for C−C and C−O bond fission of RC1 thru RC3 vary from 0.938 to 1.024, among which only the scale factors for C−O bond fission exceed 1. Figure 5 illustrates an example for bond dissociation

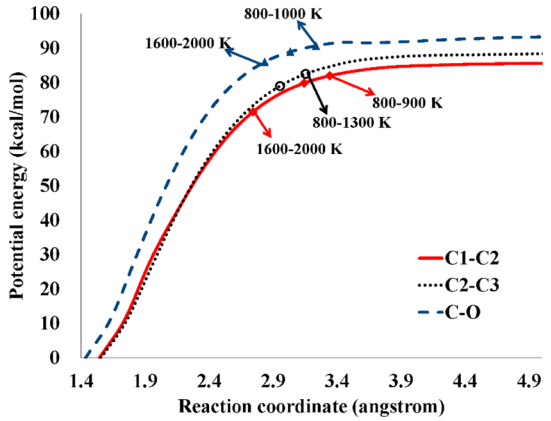

Figure 5. Minimum energy paths of bond dissociation reactions (including C1−C2, C2−C3, and C−O) of RC1. Symbols on the potential curves instruct the location of transition states determined by variational TST among the temperature range 800−2000 K.

of RC1. The MEPs of C3−C4 and C4−C5 bond cleavage are neglected for clearness since they are very close to that of C2−C3 bond cleavage. The potential energy curves for bond dissociation reactions of RC2 and RC3 are shown in the Supporting Information. The shape of the potential curve, in other words, the theoretical level used, has significant impact on the location of the transition state, consequently influencing the calculated rate constants. It will be discussed in the next section.

3.3. Rate Constants. Mere PESs calculations cannot provide enough information to describe the process of thermal decomposition of *n*-pentanol and its isomers, especially to reveal the competition between different reaction channels. Furthermore, accurate rate constants are badly needed for developing detailed chemical kinetics models of pentanol and flame.

The variational TST was used to compute the rate constants of the direct C−C and C−O bond dissociation reaction, while the transition state is located variationally with varying temperature. The low-frequency vibrational modes corresponding to the internal rotation along the breaking bonds are assumed as free rotors. To examine the validity of this assumption, we computed the hindrance potentials of these torsions by relaxed scan at various reaction coordinates using the B3LYP/6-31 g(d) method. Among all these torsions of RC1 thru RC3, no hindrance barriers exceed 200 cm^{-1}. The hindered rotor effect of the torsions with such low hindrance barriers should be neglectable. Table 2 lists the calculated high

Table 2. HPL Rate Constants of C1−C2 Scission of RC1 Varying with Temperature and Reaction Coordinate

T (K)	r = 2.754 Å	r = 2.954 Å	r = 3.154 Å	r = 3.354 Å
800	1.68×10^{-6}	6.16×10^{-7}	1.97×10^{-7}	$\mathbf{1.48 \times 10^{-7}}$
900	3.42×10^{-4}	1.59×10^{-4}	6.56×10^{-6}	$\mathbf{5.84 \times 10^{-5}}$
1000	2.42×10^{-2}	1.36×10^{-2}	$\mathbf{6.89 \times 10^{-3}}$	7.02×10^{-3}
1100	7.97×10^{-1}	5.22×10^{-1}	$\mathbf{3.15 \times 10^{-1}}$	3.56×10^{-1}
1200	1.47×10^{1}	1.09×10^{1}	**7.54**	9.43
1300	1.74×10^{2}	1.44×10^{2}	$\mathbf{1.12 \times 10^{2}}$	1.52×10^{2}
1400	1.45×10^{3}	1.32×10^{3}	$\mathbf{1.13 \times 10^{3}}$	1.64×10^{3}
1500	9.10×10^{3}	9.03×10^{3}	$\mathbf{8.47 \times 10^{3}}$	1.30×10^{4}
1600	$\mathbf{4.56 \times 10^{4}}$	4.86×10^{4}	4.93×10^{4}	7.96×10^{4}
1700	$\mathbf{1.89 \times 10^{5}}$	2.15×10^{5}	2.33×10^{5}	3.95×10^{5}
1800	$\mathbf{6.73 \times 10^{5}}$	8.08×10^{5}	9.32×10^{5}	1.64×10^{6}
1900	$\mathbf{2.09 \times 10^{6}}$	2.65×10^{6}	3.22×10^{6}	5.88×10^{6}
2000	$\mathbf{5.83 \times 10^{6}}$	7.70×10^{6}	9.85×10^{6}	1.86×10^{7}

pressure limit (HPL) rate constants $k_{HPL}(T)$ of C1−C2 scission (R1) of RC1 along the reaction coordinate as an example of the variational TST calculation. Clearly, the minimum rate constant at each temperature varies with the reaction coordinate, as shown in bold. The location of transition states for C−C and C−O dissociation of RC1 among the temperature range of 800−2000 K was illustrated in Figure 5 by various symbols on the potential curves.

Figure 6a illustrates the HPL rate constants of R1−R6 for RC1. Among the four C−C bond dissociations (R1 to R4), the rate constants of R1, R2, and R3 are very close to each other, while that of R4 (black dash dot line) is 2−15 times lower among the studied temperature range. It seems surprising since the dissociation energy of C4−C5 (δ) bond (88.3 kcal/mol) is even lower than that of C2−C3 (β) bond (89.1 kcal/mol), see Figure 2. However, from the variational TST calculation, the transition state of C4−C5 (δ) bond breaking is located at the C−C bond length being 3.3 Å (with the barrier height of 84.4 kcal/mol) when temperature varies from 800 to 1800 K, while that of C2−C3 (β) is at the bond length being 3.1 Å (with the barrier height of 82.5 kcal/mol) in the temperature range of 800−1300 K, as shown in Figure 5. This leads to the surprising difference in the calculated rate constants. Our calculations imply the importance of thorough variational TST computation for barrierless dissociation reactions, especially for the reactions with close dissociation energy. As seen from Figure 6a, another noticeable finding is the low rate constant of R6, which has the lowest barrier height, comparing to those of C−C bond dissociation reactions. Relative to the tight transition state of the H_2O elimination reaction, the transition states defined by variational TST for direct bond dissociation reactions have very low vibrational frequencies. As a result, the activation entropies of the C−C bond dissociation are much higher than that of H_2O elimination reaction (R6). Consequently, the rate constants of the C−C bond dissociations (R1−R4) are comparative to that of R6, even though R6 has a ~20 kcal/mol lower barrier height. In addition, the C−O bond fission cannot compete with the other pathways until temperature

dx.doi.org/10.1021/jp305885s | J. Phys. Chem. A 2012, 116, 9238−9244

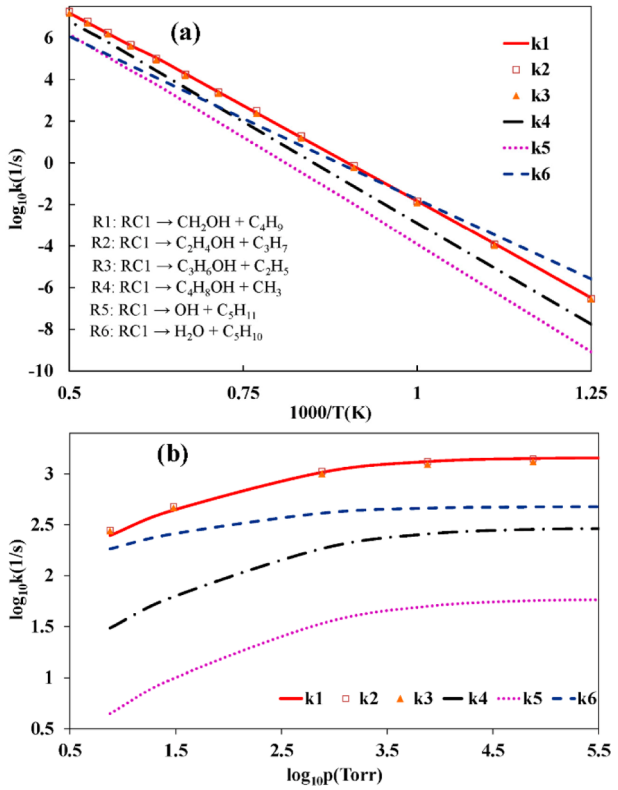

Figure 6. (a) High pressure limit and (b) pressure dependence of rate constants at 1400 K for major decomposition channels of 1-pentanol (RC1).

exceeds 1500 K. This is actually a common rule for the thermal decomposition of other alcohols including polyols.[11,28,31] The H_2O elimination channel plays a dominant role at low temperature, while the bond dissociation channels become more significant as temperature increases.

Figure 6b shows the pressure dependence of rate constants for R1−R6 of RC1 at 1400 K, which is a typical temperature for primary thermal decomposition.[10] In general, the effects of pressure falloff on the rate constants of all six reactions are not significant at 1400 K. In order to analyze the falloff behavior of these reactions, we define the parameter l as the ratio between the rate constants at 7.6×10^4 Torr and those at 7.6 Torr. The values of l for the six reactions at 1400 K are listed in Table 3.

Table 3. Falloff Behavior Analysis for RC1 at 1400 K (li Refers to the Ratio between the Rate Constant at 76,000 and 7.6 Torr for the Reaction R_i)

	$l1$	$l2$	$l3$	$l4$	$l5$	$l6$
$\langle \Delta E_{down} \rangle$ = 0.8 T	5.7	5.1	4.8	9.3	**12.7**	**2.6**
$\langle \Delta E_{down} \rangle$ = 0.4 T	10.2	8.7	8.2	18.8	27.7	3.7
increase E_a(R6) by 3000 cm^{-1}	5.4	4.8	4.5	8.7	11.8	**6.2**
decrease E_a(R5) by 2000 cm^{-1}	5.9	5.2	4.9	9.6	**7.5**	2.6

As clearly shown by Figure 6 b and Table 2, the falloff behavior of $k1$−$k6$ is controlled by their barrier heights and the competition among them. In order to gain a further insight into the falloff behavior, we artificially vary the barrier heights of R5 (showing most significant pressure dependence with the highest barrier height) and R6 (showing most insignificant pressure dependence with the lowest barrier height), then compute the parameter l again, as listed in Table 3. When we increase the barrier height of R6 by 3000 cm^{-1} (9.38 kcal/mol) and keep all other parameters unchanged, the parameter l for R6 increases dramatically from 2.6 to 6.2 (shown in bold), which implies notable increase on its falloff behavior. Similarly, when we decrease the barrier height of R5 by 2000 cm^{-1} (6.26 kcal/mol), $l5$ decreases from 12.7 to 7.5, which means the falloff behavior of R5 becomes more insignificant than before. Many experiments and practical engines are performed at 1 atm. The rate constant of each reaction at 1 atm pressure tends to depart from the high pressure limit with increasing temperature. The rate constants of R1−R5 at 1 atm are around 50%, 3% of those at HPL with temperature rising from 800 to 2000 K, while the same ratio for R6 is 100%:16%. The calculated $k(T,P)$ for decomposition channels of RC2 and RC3 are displayed in Figures 7 and 8. To avoid redundancy, the results for RC2 and RC3 will not be discussed in detail.

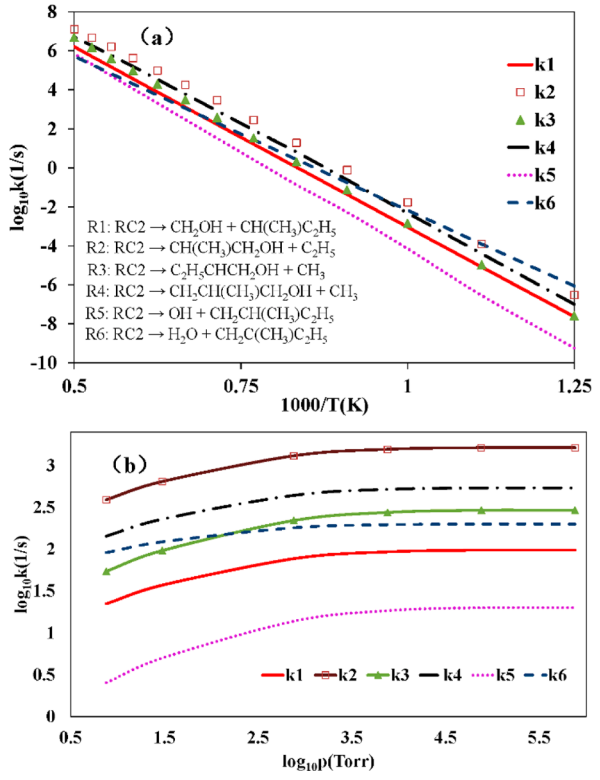

Figure 7. (a) High pressure limit and (b) pressure dependence of rate constants at 1400 K for major decomposition channels of 2-methyl-1-butanol (RC2).

The rate constants of the radical−radical recombination reactions, i.e., the reverse rate constants of the studied dissociation reactions, were deduced by the equilibrium constants K_p for the studied reactions. The Arrhenius parameters of the calculated reverse rate constants were given in Table S5 of the Supporting Information. It is as expected that the reverse rate constants show very little temperature dependence, which indirectly confirms the reliability of our calculated dissociation rate constants. We also compare the recombination rate constant of CH_2OH + t-C_4H_9 with that of a similar reaction C_2H_5 + t-C_4H_9 based on CASPT2/cc-pVDZ potential energy surfaces.[32] As shown in Figure 9, the two series of data show very similar temperature dependence, and the rate

dx.doi.org/10.1021/jp305885s | J. Phys. Chem. A 2012, 116, 9238−9244

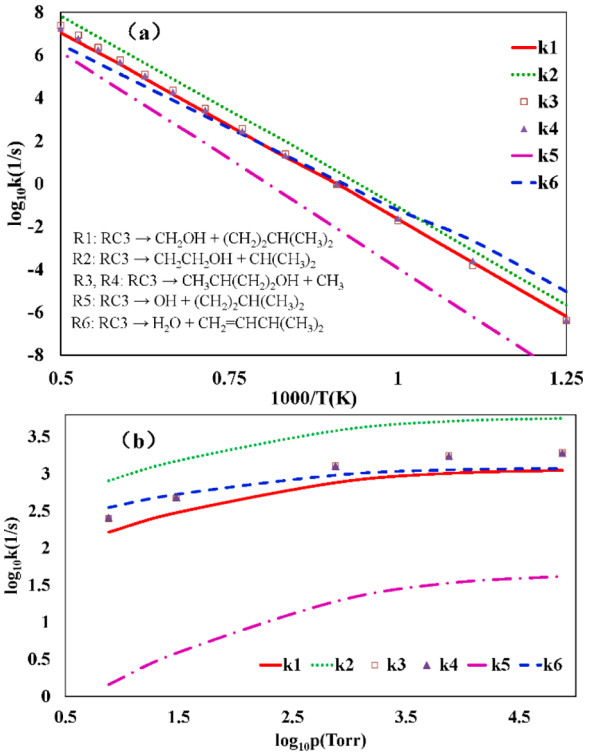

Figure 8. (a) High pressure limit and (b) pressure dependence of rate constants at 1400 K for major decomposition channels of 3-methyl-1-butanol (RC3).

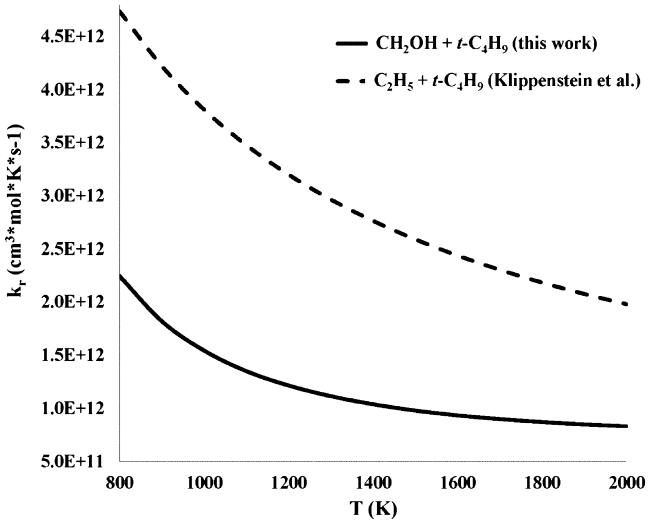

Figure 9. Comparison of the rate constant of CH_2OH + t-C_4H_9 calculated in this work with that of C_2H_5 + t-C_4H_9 computed by Klippenstein et al. (ref 32).

constant of CH_2OH + t-C_4H_9 computed in this work is around two times larger than that of C_2H_5 + t-C_4H_9 in the temperature range of 800−2000 K.

In addition, it is known that the falloff behavior of the rate constants is influenced by the collision energy transfer model. In this work, the collision energy transfer was treated using an exponential down model, while $\langle \Delta E_{down} \rangle$ was taken to be proportional to the temperature with the proportionality coefficient of 0.8 cm^{-1}/K. We also examined the effect of the proportionality coefficient on the pressure dependence of the calculated rate constants. Table 2 lists the ratio between the rate constants at 7.6×10^4 Torr and those at 7.6 Torr with using the proportionality coefficient 0.8 and 0.4 cm^{-1}/K, respectively. The falloff behavior of the six reactions is dramatically enlarged by decreasing α from 0.8 cm^{-1}/K to 0.4 cm^{-1}/K. Figure 10

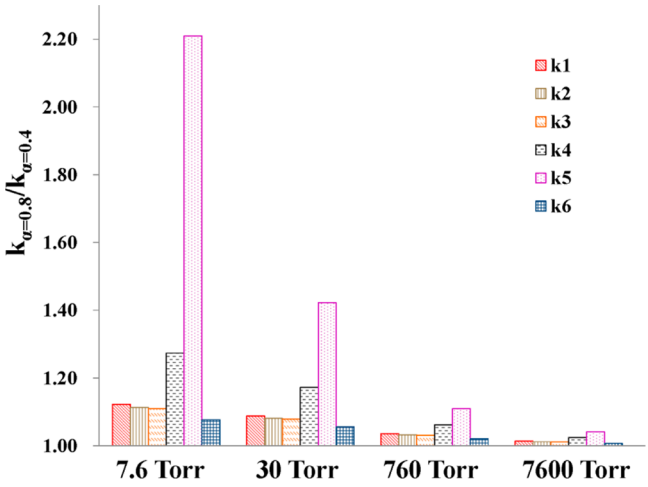

Figure 10. Effect of collisional energy transfer parameter.

illustrates the ratio of calculated rate constants by using the two proportional coefficients, i.e., $k_{\alpha=0.8}/k_{\alpha=0.4}$ for the six reactions of RC1 at various pressures. The values of $k_{\alpha=0.8}/k_{\alpha=0.4}$ for all reactions are less than 1.5, except that for R5 at 7.6 Torr, which is 2.2. We estimate that the error caused by the proportionality coefficient is within a factor of 2 for the studied reaction systems in this work. However, the accuracy of the collisional models requires further validation by kinetic modeling.

Figures for the calculated rate constants of RC2 and RC3 are shown in the Supporting Information. Finally, in the Supporting Information, the parameters A, n, and E_a of the modified Arrhenius equation $k = AT^n e^{-E_a/RT}$ for the major thermal decomposition pathways of RC1, RC2, and RC3 at various pressures (7.6, 30, 760, 7600, and 7.6×10^4 Torr and high pressure limit) are provided in Table S4.

4. CONCLUSIONS

Pentanol has been regarded as a potential biofuel with high energy density and low hygroscopicity. The fundamental research on pentanol combustion property is just started. In this work, we investigate dominant channels of thermal decomposition of three isomers of pentanol: 1-pentanol, 2-methyl-1-butanol, and 3-methyl-1-butanol by the CBS-QB3 method; subsequently, we compute the temperature- (800−2000 K) and pressure-dependent (7.6 −7.6×10^4 Torr) rate constants by the RRKM/master equation simulations. Our calculations reveal that the competition between various decomposition channels is not only controlled by the dissociation energy (or barrier heights) but also significantly influenced by entropies of the variational transition states. The H_2O elimination channel plays a dominant role at low temperature, while the bond dissociation channels become more significant as temperature increases. The kinetics of 1-pentanol decomposition was discussed in detail as an instance. The H_2O elimination channel plays a dominant role at low temperature, while the bond dissociation channels become more significant as temperature increases. At 1 atm, which is a typical experimental condition, the rate constant of H_2O elimination is close to high pressure limit when temperature is

dx.doi.org/10.1021/jp305885s | J. Phys. Chem. A 2012, 116, 9238−9244

below 1500 K, while it is only 16% of the HPL rate constant at 2000 K. However, the rate constants of the other five unimolecular reactions at 1 atm are around 50%, 3% of those at HPL with temperature varying from 800 to 2000 K. The calculated $k(T,P)$ highly depends on the accuracy of variational transition state theory. Our work provides valuable kinetic data to construct detailed chemical kinetic models for isomeric pentanol combustion.

■ ASSOCIATED CONTENT

Supporting Information

Cartesian coordinates (in Å) of all stationary points for R1 to R6 of RC1 thru RC3 at the B3LYP/6-311G(2df,d,p) level; calculated rate constants of major decomposition reactions for RC1, RC2, and RC3 at various pressures; calculated reverse rate constants of major decomposition reactions of RC1 thru RC3; minimum energy path of bond dissociation reactions of RC2 and RC3. This material is available free of charge via the Internet at http://pubs.acs.org.

■ AUTHOR INFORMATION

Corresponding Author

*E-mail: feng2011@ustc.edu.cn (F.Z.); zld@ustc.edu.cn (L.Z.).

Notes

The authors declare no competing financial interest.

■ ACKNOWLEDGMENTS

This research was supported by Natural Science Foundation of China (50925623 and 10805047), Chinese Academy of Sciences, and China Postdoctoral Science Foundation (2011M501049). The numerical calculations in this article have been carried out on the supercomputing system in the Supercomputing Center of University of Science and Technology. We thank Professor Theodore S. Dibble for helpful discussions, and the anonymous referees for their extensive contributions towards improving this work.

■ REFERENCES

(1) Demirbas, A. *Prog. Energy Combust. Sci.* **2007**, *33*, 1−18.
(2) Johnson, M. V.; Goldsborough, S. S.; Serinyel, Z.; O'Toole, P.; Larkin, E.; O'Malley, G.; Curran, H. J. *Energy Fuels* **2009**, *23*, 5886−5898.
(3) Nielsen, D. R.; Amarasiriwardena, G. S.; Prather, K. L. J. *Bioresour. Technol.* **2010**, *101*, 2762−2769.
(4) Cann, A. F.; Liao, J. C. *Appl. Microbiol. Biotechnol.* **2009**, *85*, 893−899.
(5) Yang, B.; Oßwald, P.; Li, Y. Y.; Wang, J.; Wei, L. X.; Tian, Z. Y.; Qi, F.; Kohse-Höinghaus, K. *Combust. Flame* **2007**, *148*, 198−209.
(6) Harper, M. R.; Geem, K. M. V.; Pyl, S. P.; Marin, G. B.; Green, W. H. *Combust. Flame* **2011**, *158*, 16−41.
(7) Hansen, N.; Harper, M. R.; Green, W. H. *Phys. Chem. Chem. Phys.* **2011**, *13*, 20262−20274.
(8) Veloo, P. S.; Egolfopoulos, F. N. *Proc. Combust. Inst.* **2010**, *33*, 987−993.
(9) Sarathy, S. M.; Thomson, M. J.; Togbé, C.; Dagaut, P.; Halter, F.; Mounaim-Rousselle, C. *Combust. Flame* **2009**, *156*, 852−864.
(10) Cai, J.; Zhang, L.; Yang, J.; Li, Y.; Zhao, L.; Qi, F. *Energy* **2012**, *43*, 94−102.
(11) El-Nahas, A. M.; Mangood, A. H.; Takeuchi, H.; Taketsugu, T. *J. Phys. Chem. A* **2011**, *115*, 2837−2846.
(12) Zhou, C.-W.; Simmie, J. M.; Curran, H. J. *Combust. Flame* **2011**, *158*, 726−731.
(13) Zhou, C.-W.; Simmie, J. M.; Curran, H. J. *Int. J. Chem. Kinet.* **2012**, *44*, 155−164.
(14) Seal, P.; Papajak, E.; Truhlar, D. G. *J. Phys. Chem. Lett.* **2012**, *3*, 264−271.
(15) Grana, R.; Frassoldati, A.; Faravelli, T.; Niemann, U.; Ranzi, E.; Seiser, R.; Cattolica, R.; Seshadri, K. *Combust. Flame* **2010**, *157*, 2137−2154.
(16) Black, G.; Curran, H. J.; Pichon, S.; Simmie, J. M.; Zhukov, V. *Combust. Flame* **2010**, *157*, 363−373.
(17) Mellouki, A.; Oussar, F.; Lun, X.; Chakir, A. *Phys. Chem. Chem. Phys.* **2004**, *6*, 2951−2955.
(18) Welz, O.; Zádor, J.; Savee, J. D.; Ng, M. Y.; Meloni, G.; Fernandes, R. X.; Sheps, L.; Simmons, B. A.; Lee, T. S.; Osborn, D. L.; Taatjes, C. A. *Phys. Chem. Chem. Phys.* **2012**, *14*, 3112.
(19) Togbé, C.; Halter, F.; Foucher, F.; Mounaim-Rousselle, C.; Dagaut, P. *Proc. Combust. Inst.* **2011**, *33*, 367−374.
(20) Dayma, G.; Togbé, C.; Dagaut, P. *Energy Fuels* **2011**, *25*, 4986−4998.
(21) Montgomery, J. A.; Frisch, M. J.; Ochterski, J. W.; Petersson, G. A. *J. Chem. Phys.* **1999**, *110*, 2822−2827.
(22) Montgomery, J. A.; Frisch, M. J.; Ochterski, J. W.; Petersson, G. A. *J. Chem. Phys.* **2000**, *112*, 6532−6542.
(23) Frisch, M. J.; Trucks, G. W.; Schlegel, H. B.; Scuseria, G. E.; Robb, M. A.; Cheeseman, J. R.; Montgomery, J. A., Jr.; Vreven, T.; Kudin, K. N.; Burant, J. C.; Millam, J. M.; Iyengar, S. S.; Tomasi, J.; Barone, V.; Mennucci, B.; Cossi, M.; Scalmani, G.; Rega, N.; Petersson, G. A.; Nakatsuji, H.; Hada, M.; Ehara, M.; Toyota, K.; Fukuda, R.; Hasegawa, J.; Ishida, M.; Nakajima, T.; Honda, Y.; Kitao, O.; Nakai, H.; Klene, M.; Li, X.; Knox, J. E.; Hratchian, H. P.; Cross, J. B.; Bakken, V.; Adamo, C.; Jaramillo, J.; Gomperts, R.; Stratmann, R. E.; Yazyev, O.; Austin, A. J.; Cammi, R.; Pomelli, C.; Ochterski, J. W.; Ayala, P. Y.; Morokuma, K.; Voth, G. A.; Salvador, P.; Dannenberg, J. J.; Zakrzewski, V. G.; Dapprich, S.; Daniels, A. D.; Strain, M. C.; Farkas, O.; Malick, D. K.; Rabuck, A. D.; Raghavachari, K.; Foresman, J. B.; Ortiz, J. V.; Cui, Q.; Baboul, A. G.; Clifford, S.; Cioslowski, J.; Stefanov, B. B.; Liu, G.; Liashenko, A.; Piskorz, P.; Komaromi, I.; Martin, R. L.; Fox, D. J.; Keith, T.; Al-Laham, M. A.; Peng, C. Y.; Nanayakkara, A.; Challacombe, M.; Gill, P. M. W.; Johnson, B.; Chen, W.; Wong, M. W.; Gonzalez, C.; Pople, J. A. *Gaussian 03*, Revision D.01; Gaussian, Inc.: Wallingford, CT, 2003.
(24) Linstrom, P. J.; Mallard, W. G. *NIST Chemistry Webook*; National Institute of Standards and Technology: Gaithersburg MD.
(25) Mokrushin, V.; Bedanov, V.; Tsang, W.; Zachariah, M.; Knyazev, V. In *ChemRate*, version 1.5.2; National Institute of Standards and Testing: Gaithersburg, MD, 2006.
(26) da Silva, G.; Bozzelli, J. W. *J. Phys. Chem. A* **2008**, *112*, 3566−3575.
(27) Welty, J. R.; Wicks, C. E.; Wilson, R. E.; Rorrer, G. L. *Fundamentals of Momentum, Heat and Mass Transfer*, 4th ed.; John Wiley and Sons Ltd.: New York, 2001.
(28) Ye, L.; Zhao, L.; Zhang, L.; Qi, F. *J. Phys. Chem. A* **2011**, *116*, 55−63.
(29) Park, J.; Zhu, R. S.; Lin, M. C. *J. Chem. Phys.* **2002**, *117*, 3224−3230.
(30) Bui, B. H.; Zhu, R. S.; Lin, M. C. *J. Chem. Phys.* **2002**, *117*, 11188−11195.
(31) Ye, L.; Zhang, F.; Zhang, L.; Qi, F. *J. Phys. Chem. A* **2012**, *16*, 4457−4465.
(32) Klippenstein, S. J.; Georgievskii, Y.; Harding, L. B. *Phys. Chem. Chem. Phys.* **2006**, *8*, 1133−1147.